Available online at www.sciencedirect.com
SCIENCE DIRECT®
Journal of Hydrology 283 (2003) 281–289
Journal of Hydrology
www.elsevier.com/locate/jhydrol

A model comparison of karst aquifer evolution for different matrix-flow formulations

Georg Kaufmann

Institute of Geophysics, University of Göttingen, Herzberger Landstrasse 180, 37075, Göttingen, Germany

Received 17 September 2002; accepted 14 July 2003

Abstract

The evolution of permeability and flow in a karst aquifer is studied by numerical simulations. The aquifer considered consists of a large central fracture, a network of finer fissures, and a porous rock matrix. Enlargement of both the central fracture and the fissures by chemical dissolution is possible, hence the conductivities in the fracture and the fissure system can increase with time. No dissolution is allowed in the porous rock matrix, which has a constant conductivity. Flow is driven by a simple fixed head boundary condition representative for the initial phase of karstification. A systematic parameter study is carried out by varying the initial width of the fissure network and the conductivity of the rock matrix, while keeping the initial width of the central fracture fixed. Key parameters such as flowrates, breakthrough times, and conductivities for the different models are compared. If either the conductivity of the rock matrix is high enough or the initial width of the fissures is large enough to carry flow, breakthrough times of the aquifer are significantly reduced, when compared to a model with low matrix conductivity and small fissures. However, due to the dissolutional widening of fissures the evolution of the aquifer is distinctively different for models with rock matrix simulated by a porous medium or a fissure network.

Keywords: Karst; Limestone; Dissolution; Triple-porosity

1. Introduction

Flow and transport through a karst aquifer is strongly depending on heterogeneities, as fractures enlarged by chemical dissolution provide preferential flowpaths, which respond quickly to recharge events in the catchment area. However, the distribution and geometry of fractures in a karst aquifer is difficult to access by direct observation. Here, numerical modelling of the evolution of flow in a karst aquifer is a useful tool to study the impact of strong heterogeneities in permeability. Several models have been developed in the last decade to simulate the evolution of fractures and flow in karst aquifers (e.g. Groves and Howard, 1994; Howard and Groves, 1995; Clements et al., 1996, 1997; Siemers and Dreybrodt, 1998; Kaufmann and Braun, 1999, 2000; Gabrovšek et al., 2000). The basis of all of these models is a network of interconnected fractures, which are enlarged by chemical dissolution. Flow is driven by boundary conditions simulating simple aquifer models. However, differences in the models arise from the treatment of flow in the rock matrix

E-mail address: gkaufman@uni-geophys.gwdg.de (G. Kaufmann)

0022-1694/$ - see front matter © 2003 Elsevier B.V. All rights reserved.
doi:10.1016/S0022-1694(03)00270-1

between the fractures. While the models of Groves and Howard (1994) and Kaufmann and Braun (1999) only consider the fracture network, the matrix component is modelled as porous continuum in the models of Clemens et al. (1996), Bauer et al. (1999) (Tübingen model) and Kaufmann and Braun (1999) (Göttingen model). In the latter models, the dissolutional widening in the porous continuum is not taken into account. The model from Siemers and Dreybrodt (1998) and Gabrovšek et al. (2000) (Bremen model) describes the rock matrix through a dense network of narrow fissures, onto which the fracture network is superimposed. This model allows for dissolution both in the finer fissures simulating the matrix and the more prominent fractures.

For both the Tübingen model (Bauer et al., 2000) and the Bremen model (Romanov et al., 2002) a benchmark scenario has been published. In this article, we apply the benchmark scenario to the Göttingen model, and we simulate a karst aquifer with three different components: a prominent fracture embedded into a network of smaller fissures and porous matrix. Hence our model has three characteristic porosities. We are thus able to simulate flow and evolution in the early phase of a karst aquifer, with flow initially controlled by the fracture and the porous matrix, and subsequently by the enlargement of smaller fissures in the system.

2. Theory

The benchmark scenario represents an idealised karst aquifer, with a horizontal limestone layer 742.5 m in length and 375 m wide (Fig. 1). The aquifer is discretised into 100×51 nodes, and the fine fissure system has fissures with a fissure spacing of 7.5 m. A larger fracture is located in the center of the karst aquifer. While the large fracture has an initial diameter of 0.2 mm, the initial fissure diameter is varied between 0.01 and 0.2 mm. In between the fissures the matrix is simulated as porous continuum, and the matrix conductivity is varied from 10^{-15} to 10^{-3} m/s. Flow in the karst aquifer is driven by a fixed head boundary condition, with heads fixed to 100 m along the left side, and 0 m along the right side. Both the upper and lower boundaries are no-flow boundaries. Other model parameter values are listed in Table 1.

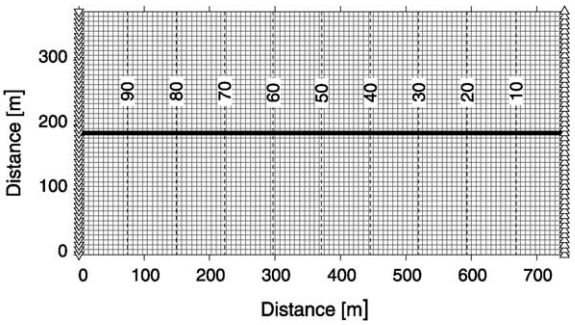

Fig. 1. Geometry of the model domain. Fissures are shown as thin lines, the prominent fracture as thick line. The dashed contour lines depict the initial head distribution. Inverted triangles indicate the 100 m fixed head along the left side, normal triangles the 0 m head along the right side. Other boundaries are no-flow boundaries.

Flow in the fractured, porous karst aquifer is modelled by the steady-state continuity equation without recharge

$$\frac{\partial}{\partial x}\left(bK\frac{\partial h}{\partial x}\right)+\frac{\partial}{\partial y}\left(bK\frac{\partial h}{\partial y}\right)=0. \quad (1)$$

Table 1
Reference model parameters

Parameter	Description	Unit	Value
K_m	Matrix conductivity	m/s	$10^{-15}-10^{-3}$
d_f	Fissure width	mm	$0.01-0.2$
d_c	Fracture width	mm	0.2
δ	Fracture spacing	m	7.5
ρ	Calcite density	kg/m^3	2700
m_r	Calcite atomic mass	g/mol	100.1
g	Gravitational acceleration	m/s^2	9.81
ν	Kinematic viscosity	m^2/s	1.14×10^{-6}
n_1	Linear exponent	–	1
n_2	Non-linear exponent	–	4
k_0	Dissolution-rate constant	mol/m^2/s	4×10^{-7}
D	Diffusion constant	m^2/s	10^{-9}
c_i	Initial calcium concentration	mol/m^3	0
c_s	Threshold calcium concentration	mol/m^3	$0.9c_{eq}$
c_{eq}	Equilibrium calcium concentration	mol/m^3	2
t	Time step	yr	1

Here, x and y are the northward and eastward coordinate directions, h is the hydraulic head in the model domain, K and b are the conductivity and the aquifer thickness. The transmissivity $T = bK$ controls the flow, hence for simplicity we choose a nominal aquifer thickness of $b = 1$ m. For a total of N nodes in the model domain, (1) represents a set of N equations for the N unknown heads h_i at nodes i. The conductivity in the porous matrix K_m remains constant throughout the evolution, while the conductivities in the fracture and the fissures $K_c = K_c(t)$ increases with time due to the enlargement of the elements by chemical dissolution:

$$K_c(t) = \frac{g}{32\nu} d(t)^2. \tag{2}$$

Here, g is gravitational acceleration, ν the kinematic viscosity of water, t is time, and $d(t)$ the time-dependent diameter of the fractures and fissures.

The diameter increases with time, depending on the calcium fluxrate $F_{Ca^{2+}}$ in the element

$$d(t_i) = d(t_{i-1}) + \frac{F_{Ca^{2+}} m_r}{\rho}(t_i - t_{i-1}), \tag{3}$$

with m_r and ρ the atomic mass and the density of calcite. The calcium fluxrate depends on the actual concentration c of calcium in the solution with respect to the equilibrium concentration c_{eq} (e.g. Buhmann and Dreybrodt, 1985a,b; Dreybrodt, 1988; Svensson and Dreybrodt, 1992; Eisenlohr et al., 1999),

$$F_{Ca^{2+}} = k_i \left(1 - \frac{c}{c_{eq}}\right)^{n_i}, \quad i = 1, 2, \tag{4}$$

where $c_{eq} = 2$ mol m^{-3} is the equilibrium concentration. Below a threshold ($c \leq c_s$), the fluxrate is a linear function of the calcium concentration:

$$n_1 = 1, \qquad k_1 = k_0 \left(1 + \frac{k_0 d(t)}{6 D c_{eq}}\right)^{-1}, \tag{5}$$

with the rate coefficient $k_0 = 4 \times 10^{-7}$ mol m^{-2} s^{-1}, and the diffusion coefficient $D = 10^{-9}$ m^2 s^{-1}. For small film thicknesses below 1 mm, the calcium fluxrate is mainly controlled by the surface processes at the solution–limestone boundary. For larger film thicknesses, the second term on the right-hand side of Eq. (5) becomes important, as transport processes become rate limiting. Above the threshold ($c > c_s$), a fourth-order power-law applies

$$n_2 \simeq 4, \qquad k_2 = k_1 \left(1 - \frac{c_s}{c_{eq}}\right)^{(n_1 - n_2)}. \tag{6}$$

Note that $k_2 \sim 4 \times 10^{-4}$ mol m^{-2} s^{-1} is several orders of magnitude larger than k_1, but the high-order fluxrate above the threshold remains much smaller than the low-order fluxrate valid for smaller calcium concentrations due to the power-law introduced by $n_2 = 4$ in Eq. (4). Water entering the model domain along the left side is aggressive ($c = 0$ mol m^{-3}), water leaving the porous matrix is saturated ($c = c_{eq}$). At the intersections of fractures and fissures, instantaneous and complete mixing of incoming water is assumed.

Eq. (1) is solved with a Galerkin finite element method, with triangular elements for the porous matrix and linear elements for fractures and fissures. As flow in the fractures and fissures increases with time, the flow regime can change from laminar to turbulent conditions. In that case, flow needs to be recalculated for the turbulent elements. Details of the numerical implementation and the modelling of the dissolutional widening can be found in Kaufmann and Braun (1999, 2000), and key parameters are summarised in Table 1.

3. Results

We first discuss results for three representative model runs. In Fig. 2, the widening corresponding to fracture and fissure enlargement and the hydrostatic head distribution is shown for two times. The times are chosen shortly before the breakthrough and after breakthrough. With breakthrough we define the dramatic increase in flowrate out of the right model boundary, which occurs after the establishment of linear kinetics in the entire karst aquifer. In all models discussed the central fracture has widened to around 1 m after 1000 years of evolution.

3.1. Fracture and fissure enlargement

The first model chosen is essentially a single fracture model: The central fracture with its initial width of $d_c = 0.2$ mm has an initial conductivity of

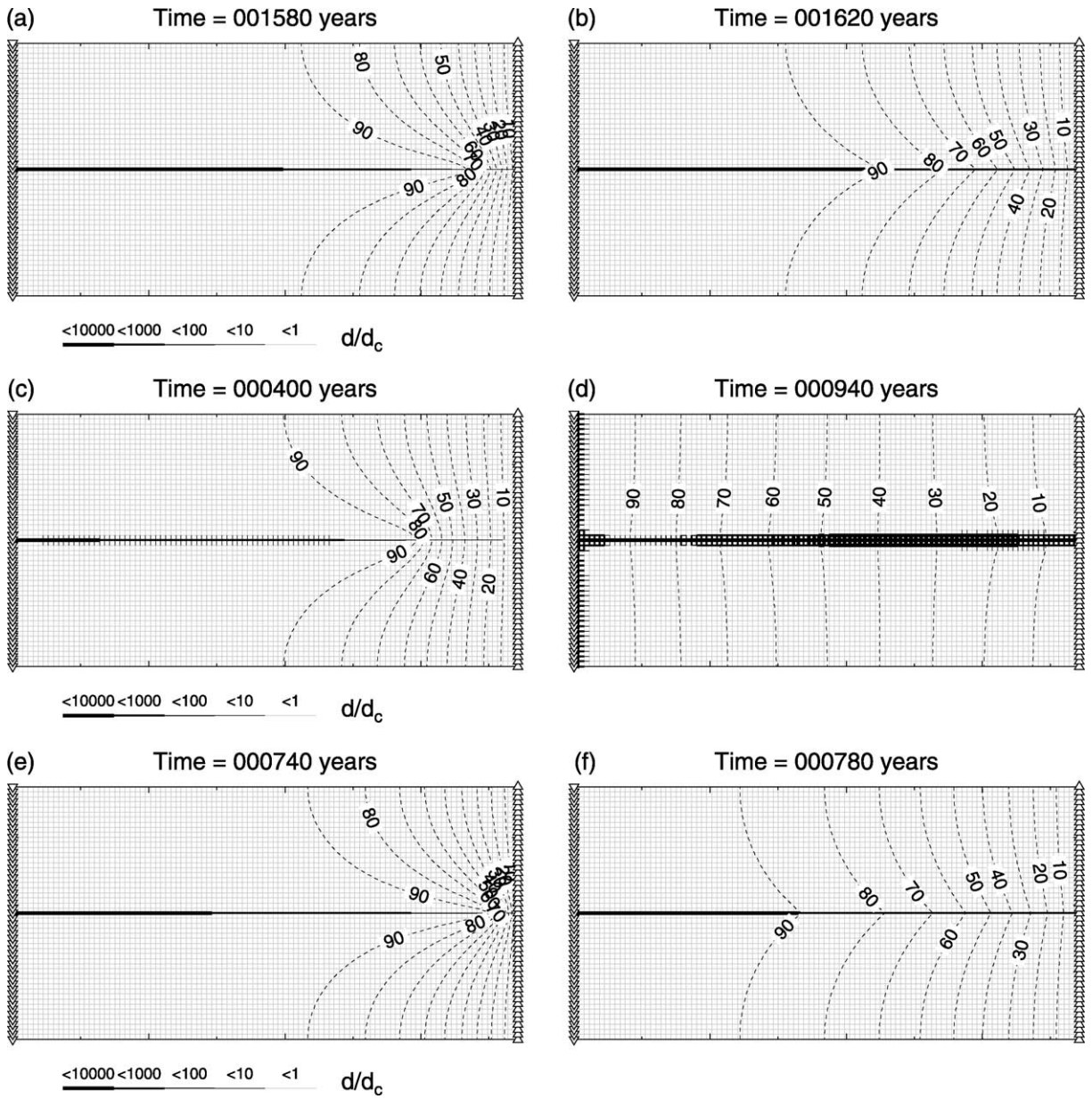

Fig. 2. Width of fissures and fractures in the karst aquifer (in m) and hydraulic head distribution (contour lines, in m) for three models. Shown is always a scenario shortly before breakthrough (left columns) and after breakthrough (right columns). Top: $d_c = 0.2$ mm, $d_f = 0.01$ mm, $K_m = 10^{-15}$ m/s. Middle: $d_c = 0.2$ mm, $d_f = 0.10$ mm, $K_m = 10^{-15}$ m/s. Bottom: $d_c = 0.2$ mm, $d_f = 0.01$ mm, $K_m = 10^{-4}$ m/s.

$K_c \simeq 1 \times 10^{-2}$ m/s, the fissures with their small initial width of $d_f = 0.01$ mm have conductivities around $K_f \simeq 3 \times 10^{-5}$ m/s, which is several orders of magnitude lower. The matrix conductivity with $K_m = 10^{-15}$ m/s is even lower. The high hydraulic head initiates enlargement of the fracture on the left side, and the enlargement propagates along the central fracture towards the right (Fig. 2(a)). As the hydraulic gradient along the enlarged part of the fracture is low, pressure contour lines are shifted to the right,

increasing the gradient along the right side. Shortly after 1600 years the breakthrough of the central fracture occurs, and the pressure lines rebound (Fig. 2(b)), as flow is now confined to the central fracture. Due to the very small fissure width, no significant enlargement in the fissure system is observed.

In the second model the initial fissure width is increased to $d_f = 0.10$ mm, which results in conductivities of the fissure system of around $K_f \simeq 3 \times 10^{-3}$ m/s. Both initial fracture and matrix conductivities are as in the first run. Again, enlargement is initiated along the left side (Fig. 2(c)), but breakthrough occurs much earlier after only 400 years. This is a result of the increased conductivity within the aquifer due to the fine fissure system. Already before breakthrough, fissures close to the central fracture are enlarged, as close to the pressure front undersaturated water is now injected into the fissure system. After breakthrough (Fig. 2(d)), the pressure lines rebound again, and a fringe of fissures around the central fracture is enlarged, creating a highly permeable zone in the center part of the aquifer.

In the third model, we set the conductivity of the fissure system low again ($d_f = 0.01$ mm, $K_f \simeq 3 \times 10^{-5}$ m/s), but this time we increase the matrix conductivity to $K_m = 10^{-4}$ m/s. Hence the permeability of the aquifer is similar to the second model, but now no enlargement takes place in the matrix. Again, the central fracture enlarges, starting on the left side (Fig. 2(e)), and pressure lines are shifted to the right. However, already after 740 years the breakthrough of the central fracture occurs, pressure lines rebound (Fig. 2(f)), and at the end of the calculation they are almost perpendicular to the central fracture. Hence the flow injected into the porous matrix results in an increase of undersaturated water flowing through the central fracture, and thus a faster enlargement.

In summary, we have shown that both modelling concepts for the matrix flow system, considering fissures as the matrix (as in the Bremen model), or modelling the matrix as a porous continuum (as in the Tübingen model), will reduce the breakthrough time of the aquifer significantly. The reason in both cases is the increased permeability of the matrix component, which will carry flow during the very early evolution of the aquifer and thus enhance dissolution in the central fracture.

3.2. Flowrates

Next, we discuss flowrates out of the right side of the aquifer more in detail. In Fig. 3(a), flowrates as a function of time are shown for models with a central fracture of $d_c = 0.2$ mm initial width, a negligible porous matrix ($K_m = 10^{-15}$ m/s), and a fissure system, for which the initial widths are varied. For very low initial fissure widths ($d_f = 0.01$ mm), flowrates increase only slowly for most of the time shown, and breakthrough occurs late around 1600 years. At breakthrough, flowrates then increase dramatically by several orders of magnitude. Increasing the initial fissure width to $d_f = 0.1$ mm, more flow can be channelled through the fissure system, and breakthrough time is reduced to 400 years. For even wider initial fissure width ($d_f = 0.15–0.17$ mm), flow through the fissure system becomes comparable to flow through the central fracture. Consequently, breakthrough occurs much earlier (300 years), and due to the enlargement of the fissure system flowrates become larger than in the single fracture case. Making the initial fissure width equal to the initial width of the central fracture ($d_c = d_f = 0.2$ mm) increases the flowrate through the aquifer from the beginning, but breakthrough in this case is delayed to around 1600 years, which is comparable to the models with very small initial fissure widths. The reason for this behaviour has already been discussed by Romanov et al. (2002): if both the fissures and the fractures have the same initial width, they essentially evolve as parallel single fractures. Exchange between horizontal fissures and fractures is negligible, and thus the breakthrough time increases to values close to the single fracture case!

In Fig. 3(b), the evolution of flowrates is shown for models with a central fracture of $d_c = 0.2$ mm initial width, a negligible fissure system ($d_f = 0.01$ mm), and different porous matrix conductivities. We observe a similar shift to lower breakthrough times, if the matrix conductivity is increased from $K_m = 10^{-15}$ to 10^{-3} m/s, which is a consequence of the increased flow through the aquifer. Significant reductions in breakthrough time are, however, limited to matrix conductivities above $K_m > 10^{-6}$ m/s.

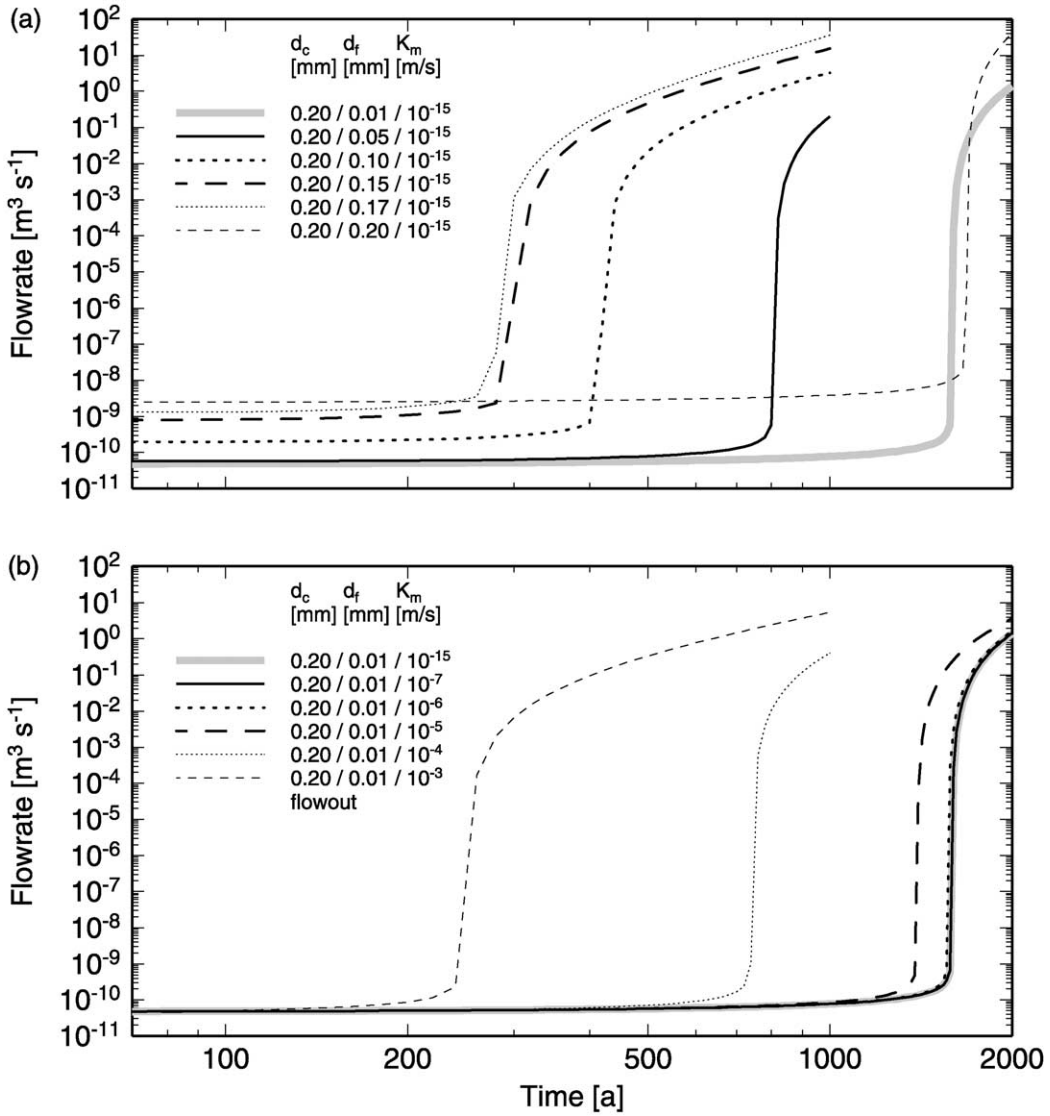

Fig. 3. Flowrates leaving the model domain through the right side. (a) Flowrates for models with prominent fractures (0.2 mm) and a fissure system width varying between 0.01 and 0.2 mm. The matrix conductivity is fixed to 10^{-15} m/s and thus negligible. (b) Flowrates for models with prominent fractures (0.2 mm) and a fixed fissure system (0.01 mm). The matrix conductivity varies between 10^{-15} and 10^{-3} m/s.

The reason for this behaviour can be found by comparing matrix and fissure conductivities: For $d_f = 0.01$ mm a fissure conductivity of around $K_f = 3 \times 10^{-5}$ m/s arises, hence the conductivity of the porous matrix needs to be at least of equal magnitude to capture a significant amount of flow.

In the Tübingen model, Bauer et al. (2000) have found that varying the exchange coefficient used to control flow between the conduit and the matrix system over a large range does not affect the breakthrough times significantly. This result is in agreement with our porous matrix models, when the matrix conductivity is below $K_m \leq 10^{-6}$ m/s. The reason for this is the difficulty to transfer water from the fractures into the porous continuum. However, we have shown that for more permeable matrices, breakthrough times are reduced, because then the porous continuum acts as a sink.

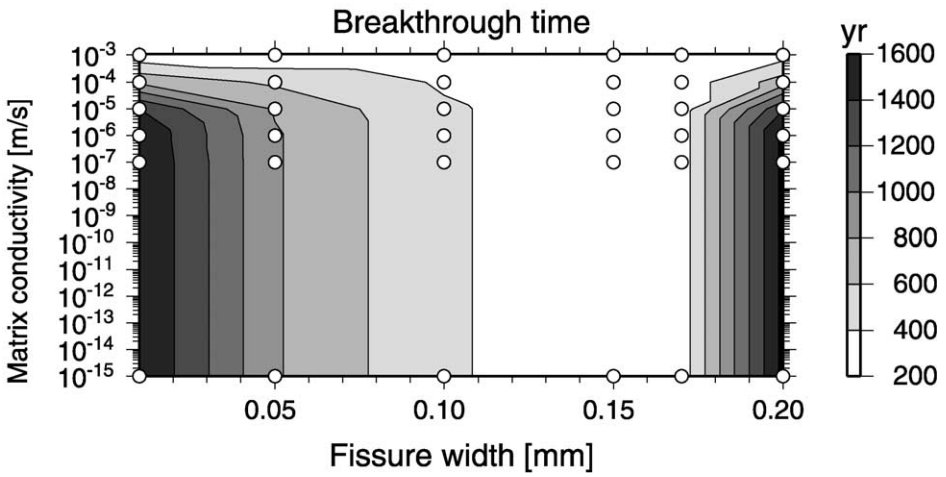

Fig. 4. Breakthrough times of fractures in the karst aquifer as a function of initial fissure width and matrix conductivity. Breakthrough times are contoured, white dots indicate models calculated.

3.3. Breakthrough times

In Fig. 4, we discuss the dependence of breakthrough times of the initial fissure widths and the porous matrix conductivity. We first focus on the models with negligible matrix conductivity ($K_m = 10^{-15}$ m/s). In these cases, breakthrough times vary from around 1600 years for models with small initial fissure width ($d_f = 0.01$ mm) to less than 300 years, if the initial fissure width is in the order of $d_f = 0.15$–0.17 mm. If $d_f \simeq d_c$, the breakthrough time increases again, as the model essentially behaves as a set of single conduits. If we allow for more permeable matrix conductivities in the range of $K_m = 10^{-7}$–10^{-3} m/s, breakthrough times are significantly reduced for small initial fissure widths, as in these cases the porous matrix is competitive enough to capture flow. For fissure widths around $d_f \sim 0.10 - 0.15$ mm, the fissured matrix is always more effective the the porous matrix and hence controls breakthrough behaviour.

3.4. Flow velocities

We finally discuss flow velocities in the aquifer shortly before breakthrough for two models. In Fig. 5(a), the matrix conductivity ($K_m = 10^{-15}$ m/s) is negligible, but the fissure width is with $d_f = 0.10$ mm large enough to capture flow. As it can be seen in the figure, flow from the central fracture is injected into the fissured system. Injection rates are largest where the central fracture width is changing from already enlarged to still small (middle section). Flow in the fissured system is then diverted through the finer fissures towards the base level. In Fig. 5(b), matrix conductivity is large ($K_m = 10^{-4}$ m/s) and competitive to the fissure system ($d_f = 0.01$ mm). In this case flow is also injected from the central fracture into the porous matrix, which then drains towards the base level.

4. Discussion

We have modelled the breakthrough behaviour of a simple karst aquifer with imposed fixed head boundary conditions on two sides. The aquifer has three distinct parts: a large central fracture, a finer fissure system, and a porous matrix. These three parts combine the numerical models of Tübingen (fracture and porous matrix) and Bremen (fracture and finer fissure system). As the hydraulic head difference driving the flow is fairly high (100 m on the left side, 0 m of the right side), porosity within the aquifer increases quickly, and the central fracture enlarges from its initial width of $d_c = 0.2$ mm to around 1 m in less then 1000 years. We have shown that the rate of enlargement is controlled by the matrix. The more

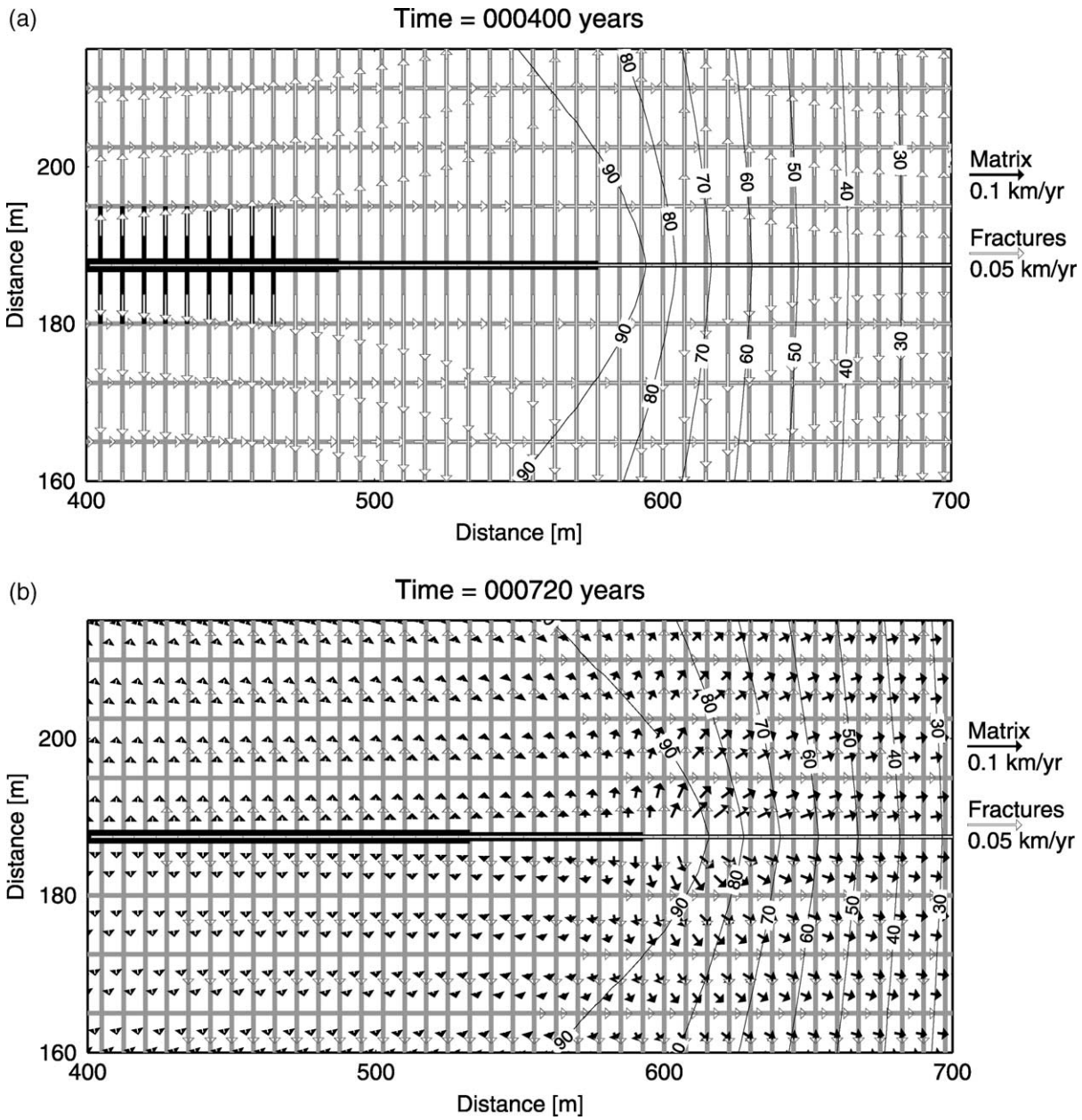

Fig. 5. Velocities in the central part of the karst aquifer shortly before breakthrough time for two models. The underlying grey and black lines are not enlarged and enlarged fractures and fissures, and contour lines depict the hydraulic head distribution. Note that flow velocities in the central fracture are so large (>10 km/yr) that no arrowheads are visible. (a) $d_c = 0.2$ mm, $d_f = 0.10$ mm, $K_m = 10^{-15}$ m/s. (b) $d_c = 0.2$ mm, $d_f = 0.01$ mm, $K_m = 10^{-4}$ m/s.

permeable the matrix is, the shorter the time until breakthrough occurs will be. For the breakthrough time, it is irrelevant if the matrix consists of a dense network of finer fissures or a porous medium. Both model scenarios will increase flow in the central fracture and thus initiate an early breakthrough. However, modelling the matrix as either a dense network of finer fissures or a porous medium will

result in different aquifer types: the porous matrix only accelerates the breakthrough of the central fracture, while keeping a constant permeability elsewhere. The network of finer fissures, on the other hand, reduces breakthrough times, but also increases porosity in the matrix by several orders of magnitude due to the dissolutional widening in the fine fissure network.

We have shown that our model can reproduce the breakthrough times and the aquifer permeability of the Bremen model (Romanov et al., 2002). In the case of the Tübingen model (Bauer et al., 2000), the results match only qualitatively, as breakthrough in the Tübingen model is significantly later due to an outdated formulation of the chemical parameter values controlling evolution.

Acknowledgements

Reviews of Rudolf Liedl and two anonymous referees have helped to improve and clarify the manuscript. The figures in this paper are drawn using the GMT graphics package (Wessel and Smith et al., 1991, 1998).

References

Bauer, S., Birk, S., Liedl, R., Sauter, M., 1999. Solutionally enhanced leakage rates of dams in karst regions. In: Palmer, A.N., Palmer, M.V., Sasowsky, I.D. (Eds.), Karst Modeling, Special Publ. 5, Karst Water Institute, Charles Town, WV, pp. 158–162.

Bauer, S., Liedl, R., Sauter, M., 2000. Modelling of karst development considering conduit-matrix exchange flow. in: Calibration and Reliability in Groundwater Modelling, Proceedings of ModelCare 99, vol. 265. IAHS Publ., Zürich, pp. 10–15.

Buhmann, D., Dreybrodt, W., 1985a. The kinetics of calcite dissolution and precipitation in geologically relevant situations of karst areas. 1. Open system. Chem. Geol. 48, 189–211.

Buhmann, D., Dreybrodt, W., 1985b. The kinetics of calcite dissolution and precipitation in geologically relevant situations of karst areas. 2. Closed system. Chem. Geol. 53, 109–124.

Clemens, T., Hückinghaus, D., Sauter, M., Liedl, R., Teutsch, G., 1996. A combined continuum and discrete network reactive transport model for the simulation of karst development. in: Calibration and Reliability in Groundwater Modelling, Proceedings of the ModelCARE 96 Conference, vol. 237. IAHS Publ., pp. 309–318.

Clemens, T., Hückinghaus, D., Sauter, M., Liedl, R., Teutsch, G., 1997. Modelling the genesis of karst aquifer systems using a coupled reactive network model. in: Hard Rock Hydrosciences, Proceedings of Rabat Symposium S2, vol. 241. IAHS Publ., pp. 3–10.

Dreybrodt, W., 1988. Processes in Karst Systems, Springer, Berlin.

Eisenlohr, L., Meteva, K., Gabrovšek, F., Dreybrodt, W., 1999. The inhibiting action of intrinsic impurities in natural calcium carbonate minerals to their dissolution kinetics in aqueous $H_2O–CO_2$ solutions. Geochem. Cosmochem. Acta 63 (6), 989–1001.

Gabrovšek, F., Menne, B., Dreybrodt, W., 2000. A model of early evolution of karst conduits affected by subterranean CO_2 sources. Environ. Geol. 39 (6), 531–543.

Groves, C.G., Howard, A.D., 1994. Early development of karst systems 1. Preferential flow path enlargement under laminar flow. Water Resour. Res. 30 (10), 2837–2846.

Howard, A.D., Groves, C.G., 1995. Early development of karst systems 2. Turbulent flow. Water Resour. Res. 31 (1), 19–26.

Kaufmann, G., Braun, J., 1999. Karst aquifer evolution in fractured rocks. Water Resour. Res. 35 (11), 3223–3238.

Kaufmann, G., Braun, J., 2000. Karst aquifer evolution in fractured, porous rocks. Water Resour. Res. 36 (6), 1381–1392.

Romanov, D., Dreybrodt, W., Gabrovsek, F., 2002. Interaction of fracture and conduit flow in the evolution of karst aquifers. In: Martin, J.B., Wicks, C., Sasowsky, I.D. (Eds.), Proceedings of the Symposium on Karst Aquifers: Florida and Related Environments, KWI Special Publ. 7, Karst Water Institute, Charles Town, WV, pp. 1–6.

Siemers, J., Dreybrodt, W., 1998. Early development of karst aquifers on percolation networks of fractures in limestone. Water Resour. Res. 34 (3), 409–419.

Svensson, U., Dreybrodt, W., 1992. Dissolution kinetics of natural calcite minerals in CO_2–water systems approaching calcite equilibrium. Chem. Geol. 100, 129–145.

Wessel, P., Smith, W.H.F., 1991. Free software helps map and display data. EOS 72, 441–446.

Wessel, P., Smith, W.H.F., 1998. New, improved version of generic mapping tools released. EOS 79, 579.